Deuterated Indocyanine Green (ICG) with Extended Aqueous Storage Shelf-Life: Chemical and Clinical Implications

Dong-Hao Li[a] and Bradley D. Smith*[a]

Abstract: Indocyanine Green (**ICG**) is a clinically approved near-infrared fluorescent dye that is used extensively for various imaging and diagnostic procedures. One drawback with **ICG** is its instability in water, which means that reconstituted clinical doses have to be used very shortly after preparation. Two deuterated versions of **ICG** were prepared with deuterium atoms on the heptamethine chain, and the spectral, physiochemical, and photostability properties were quantified. A notable mechanistic finding is that self-aggregation of **ICG** in water strongly favors dye degradation by a photochemical oxidative dimerization reaction that gives a nonfluorescent product. Storage stability studies showed that replacement of C–H with C–D decreased the dimerization rate constant by a factor of 3.1, and it is likely that many medical and preclinical procedures will benefit from the longer shelf-lives of these two deuterated **ICG** dyes. The discovery that **ICG** self-aggregation promotes photoinduced electron transfer can be exploited as a new paradigm for next-generation photodynamic therapies.

Introduction

Indocyanine green (**ICG**, Scheme 1) is the only clinically approved near-infrared (NIR) fluorescent dye with emission wavelength above 700 nm. It is commonly employed in a wide range of medical imaging and diagnostic procedures that assess cardiac output or hepatic function; visualize tissue perfusion, lymph nodes, or cancerous tissue before, during and after surgery; or visualize blood flow during ophthalmic angiography.[1–6] **ICG** is also used a great deal in preclinical research as a NIR fluorescence contrast agent for enhanced imaging of various animal models of disease. More than 5000 research papers and review articles have been published over the last five years with "indocyanine green" in the title or abstract. The recent discovery that the fluorescence emission tail of **ICG** extends beyond 1000 nm and can be detected using modern commercial cameras heralds a new set of opportunities in short wave infrared (SWIR) imaging,[7,8] and there is also considerable ongoing development of nanoscale **ICG** delivery systems for next-generation imaging and treatment strategies.[9] The clinical safety record for **ICG** over several decades is impressive,[10] and substantial growth in clinical and pre-clinical usage is expected in the coming years.

ICG is chemically stable when stored as a dry powder and the standard clinical procedure is to reconstitute it as a sterile aqueous solution immediately before patient dosage. In some cases, the formulation includes ~5% NaI.[3] The clinical dose size varies with procedure, but a common concentration in a single 3 mL aqueous bolus is 2.5 mg/mL. **ICG** binds rapidly and strongly to serum proteins and the noncovalent **ICG**/protein complexes exhibit enhanced stability and fluorescence emission at 820 nm.[11] Moreover, there is very little extravasation of the **ICG**/protein complexes from the bloodstream which enables vasculature visualization using standard biomedical NIR fluorescence imaging equipment.[12,13] Within ~20 minutes after dosing, virtually all of the **ICG**/protein complex is cleared from the bloodstream through the liver and into the bile juice without chemical modification.[14,15] Some clinical procedures, such as fluorescence guided surgery, benefit from repeated cycles of intravenous **ICG** dosing and subsequent fluorescence imaging.[14,16] A recently modified approach to fluorescence guided surgery of cancer is named "second-window ICG" and involves infusion of a high dose of **ICG** (~5.0 mg/kg) at 24 h before surgery.[17–19]

A well-known drawback with **ICG** is its propensity to degrade rapidly in aqueous solution and generate nonfluorescent by-products. For example, one study found that a solution in water had only 20% **ICG** remaining after sitting for 24 h,[20] and a rat imaging study reported almost complete loss of vasculature image if the aqueous solution was more than 24 h old.[21] Because of this rapid decrease in aqueous **ICG** purity, the FDA recommendation is to discard any unused aqueous sample within six hours of reconstitution. There is little doubt that the clinical benefit of **ICG** would be enhanced if the shelf-life of an aqueous stock solution could be extended and, not surprisingly,

[a] *D.-H. Li, Prof. B. D. Smith*
Department of Chemistry & Biochemistry
University of Notre Dame
251 Nieuwland Science Hall
Notre Dame, IN, 46545 (USA)
E-mail: smith.115@nd.edu

Supporting information for this article is available on the WWW under https://doi.org/10.1002/chem.202102816

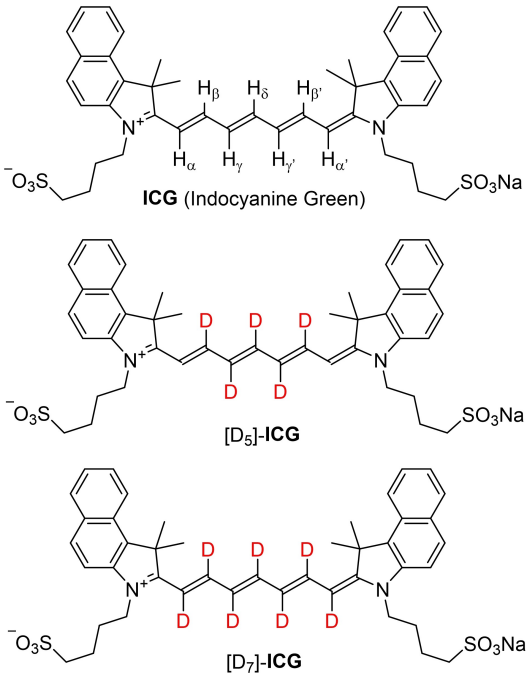

Scheme 1. Chemical structures of **ICG**, [D_5]-**ICG**, and [D_7]-**ICG**.

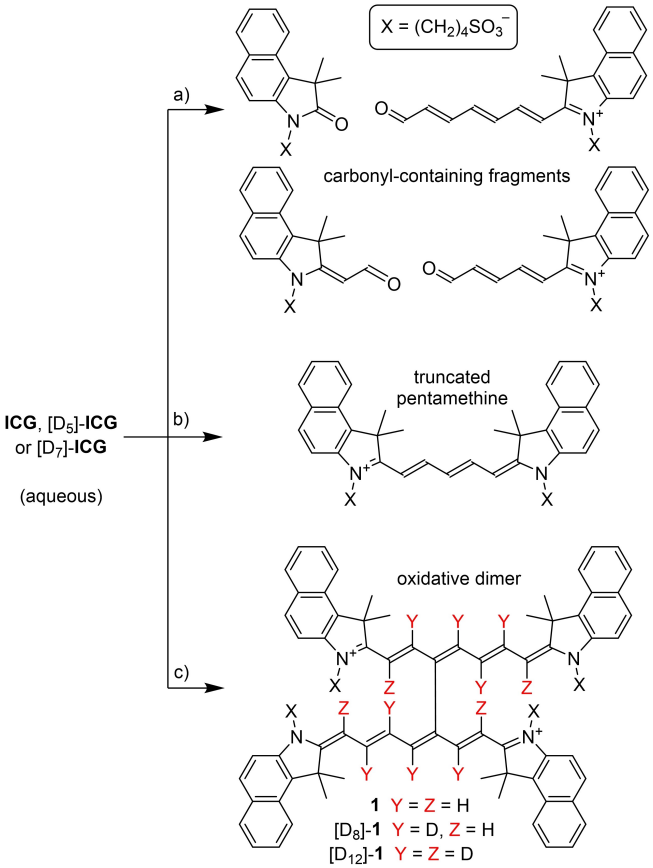

Scheme 2. Three distinct degradation pathways for aqueous **ICG** in the presence of air and light. Pathway a: double-bond cleavage to produce carbonyl-containing fragments. Pathway b: truncation to produce pentamethine homologue. Pathway c: oxidative dimerization to produce **1**.

considerable effort has been made over the years to elucidate the degradation pathway(s) and identify the contributing factors. Systematic studies of **ICG** degradation are hard to conduct because the dye has an amphiphilic molecular structure which promotes extensive self-aggregation at concentrations $>10\ \mu M$, and the aggregation alters the chemical and photophysical properties.[3,8] However, there is good evidence that the degradation of **ICG** depends on several factors, including dye concentration, the nature of the solvent, temperature, and the presence of air, light, or specific chemical additives.[3,21,22] Moreover, the combination of light and molecular oxygen promotes three chemically distinct **ICG** degradation pathways (Scheme 2). The best known pathway is a photosensitized reaction of excited state singlet oxygen with **ICG** to produce carbonyl-containing fragments that do not absorb or emit NIR light.[23,24] A second, minor photochemical process is a heptamethine truncation reaction that generates small amounts of the pentamethine homologue.[25,26] Quite recently, a third degradation process was elucidated, namely, coupling of two molecules of **ICG** to give the oxidative dimer **1**.[27,28] However, its prevalence in a stored clinical formulation (2.5 mg/mL in water) was not reported.

The general goal of this present study was to determine whether the kinetics of **ICG** degradation are altered if specific hydrogen atoms (H) on the heptamethine dye are replaced with heavier deuterium atoms (D). We reasoned that a large deuterium kinetic isotope effect would reveal valuable new chemical insight concerning the degradation mechanism, and at the same time provide a novel way to extend the shelf-life of a clinical aqueous dose. The substantial literature on deuterium kinetic isotope effects includes multiple examples of deuterated pharmaceuticals and biomolecules with enhanced chemical stability.[29] The very few reports of deuterated dyes have primarily focused on the isotope-induced changes in photophysical properties,[30] but a recent photostability study found that visible rhodamine dyes with appended deuterated alkylamino groups (auxochromes) exhibit decreased photobleaching when irradiated with intense light.[31,32] Here, we demonstrate enhanced stability using a very different deuterium substitution strategy that has not been described before; that is, direct deuteration of a near-infrared polyene chromophore. We describe the synthesis of two novel deuterated analogues of **ICG**, specifically [D_5]-**ICG** and [D_7]-**ICG** (Scheme 1) and a comparison of spectral and chemical stabilities that reveals a threefold reduction in the rate of degradation in aqueous solution, leading to extended shelf-life of stock solutions that match the clinical formulation. The results suggest that switching to deuterated **ICG** is likely to mitigate the 60-year clinical problem of aqueous **ICG** instability.

Results and Discussion

Synthesis and aqueous stability studies

We decided that direct deuteration of **ICG** to make [D_5]-**ICG** or [D_7]-**ICG** was not possible,[33,34] and that a more feasible approach was to exploit a recently refined method to make heptamethine cyanine dyes via Zincke salts as reaction intermediates.[35–38] Using this versatile process we prepared [D_5]-**ICG** and [D_7]-**ICG** on a large scale using the chemical reactions in Scheme 3. The key intermediate is the Zincke salt **2**, derived from cheap and readily available [D_5]pyridine.[39,40] Separate transimination reactions provided the linear dianil intermediates **4** or **5** which were not isolated but condensed in situ with indolenium **3** to give [D_5]-**ICG**. Alternatively, conversion of [D_5]-pyridine into isolable [D_5]glutaconaldehyde, **6**,[41] offered a third successful path to [D_5]-**ICG**. These three different synthetic methods provide broad reactivity scope for future efforts to make additional heptamethine dyes with deuterated polymethines. To make [D_7]-**ICG**, the solvent was simply switched to CH_3OD which enabled deuterium exchange with the acidic methyl protons on indolenium **3** to generate [D_3]-**3** in situ. The number of peaks and peak splitting patterns within the ^{1}H spectra of [D_5]-**ICG** and [D_7]-**ICG** were consistent with their >99% isotopically labeled structures. Moreover, the ^{1}H spectra showed that stock solutions of [D_5]-**ICG** and [D_7]-**ICG** sitting in H_2O for one month do not undergo any measurable amount of deuterium/hydrogen exchange. In summary, the technically straightforward and scalable syntheses of [D_5]-**ICG** and [D_7]-**ICG** combined with the enhanced shelf-life (see below) make them economically attractive options for immediate employment in preclinical research or future development for clinical applications.

The photophysical properties of **ICG**, [D_5]-**ICG** and [D_7]-**ICG** are listed in Table 1. To ensure no spectral artefacts due to differences in synthetic methods, all three dyes were prepared and purified by homologous procedures. In DMSO, the solutions of [D_5]-**ICG** and [D_7]-**ICG** were found to be ~30% brighter than an equivalent solution of **ICG**, but in fetal bovine serum (FBS) there was essentially no difference in fluorescence brightness. We speculate that the brightness increase of free monomeric dye in DMSO is due to diminished non-radiative decay since C–D bonds have significantly lower vibrational energy ($\nu \approx 2200\ cm^{-1}$) than C–H bonds ($\nu \approx 3000\ cm^{-1}$) and that the effect is lost when the dye is associated with serum proteins.

The relative stabilities of aqueous **ICG**, [D_5]-**ICG**, and [D_7]-**ICG** were assessed under two distinctly different conditions. The first set of studies were high photon intensity photobleaching experiments that mimicked clinical imaging or diagnostic conditions that fragment the **ICG** and produce non-fluorescent carbonyl-containing compounds (pathway A in Scheme 2).[23,24] That is, the dye concentration was low (2 μM), the photon flux was continuous and high, and the samples were exposed to air.

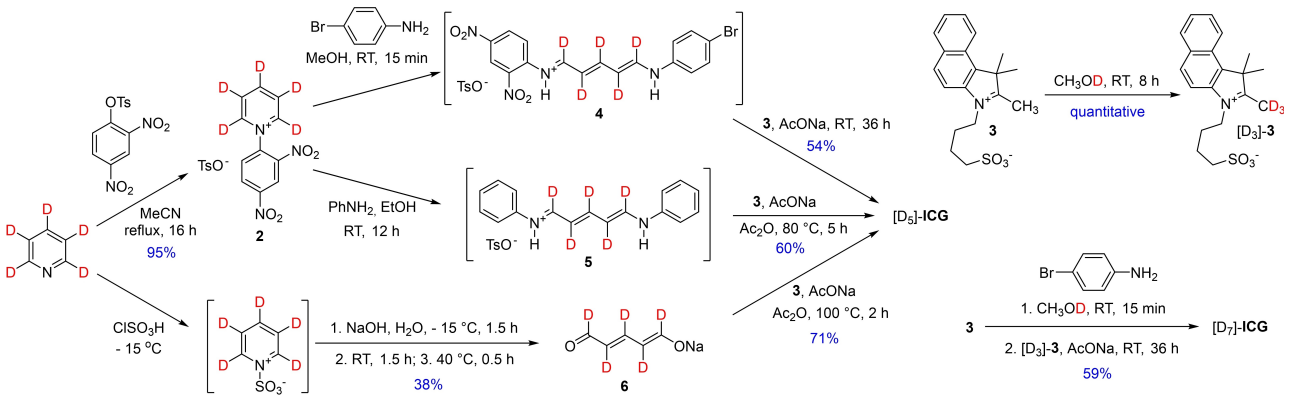

Scheme 3. Syntheses of [D_5]-**ICG** and [D_7]-**ICG**.

Table 1. Photophysical properties at room temperature.

Dye	Solvent[a]	λ^{abs}_{max} [nm]	λ^{em}_{max} [nm]	ε [$M^{-1}cm^{-1}$]	R^2	Φ_F [%][b]	Brightness[c]
ICG	DMSO	795	820	224 000	0.999	16.7 ± 0.6	37 000
ICG	FBS	800	813	197 000	0.998	9.7 ± 0.4	19 000
[D_5]-**ICG**	DMSO	793	819	253 000	0.999	19.8 ± 0.5	49 000
[D_5]-**ICG**	FBS	796	813	205 000	0.997	10.5 ± 0.3	21 000
[D_7]-**ICG**	DMSO	794	818	228 000	0.999	20.8 ± 0.5	48 000
[D_7]-**ICG**	FBS	796	812	200 000	0.999	10.3 ± 0.4	21 000
1	DMSO	787	820	327 000	0.999	0.12 ± 0.06	390
1	FBS	796	820	256 000	0.998	0.12 ± 0.04	310

[a] DMSO = dimethylsulfoxide; FBS = fetal bovine serum. Dye concentration range is 0–5 μM. All measurements conducted at room temperature. [b] For all **ICG** derivatives, absolute fluorescence quantum yield measured directly by photon counting. For **1**, the measurements are relative to **ICG** in DMSO. [c] Brightness = ε × quantum yield, error is ± 15%.

An intense light source (xenon lamp) was used to simultaneously illuminate separate solutions of the three dyes (each 2.0 μM in PBS), and the changes in NIR absorption spectra were monitored over time. The curves in Figure S15 (Supporting Information) show that all three dye solutions exhibited essentially the same rate of photobleaching. A repeat experiment examined the three dyes in FBS and observed a slower rate of photobleaching (consistent with the known protection of **ICG** due to noncovalent association with the albumin, globulin, and lipoprotein in FBS) with no difference between the dyes.[11] In other words, the photobleaching experiments indicated no significant deuterium kinetic isotope effect, a finding that is consistent with two literature facts: a) the mechanism for **ICG** photobleaching under high photon intensity illumination conditions (Scheme S1) is cycloaddition with photogenerated singlet oxygen and formation of unstable dioxetane intermediates that fragment to produce the carbonyl-containing compounds,[23,24,42,43] and b) dioxetane fragmentation is known to exhibit a negligible secondary deuterium kinetic isotope effect.[44]

The second set of dye stability experiments were designed to mimic the low photon intensity storage conditions experienced by a typical reconstituted dose in water before it is administered in a clinical setting. Thus, stock solutions of the dyes were exposed to the atmosphere and laboratory lights during the initial reconstitution and periodic sampling, but otherwise stored as capped vials in the dark at room temperature. Most literature studies on the stability of aqueous **ICG** have focused on relatively dilute solutions (< 50 μg/mL),[20,28,45,46] and very few studies have examined aqueous **ICG** solutions at the higher concentrations that match a reconstituted clinical dose (e.g., 1.0–2.5 mg/mL).[47] The water solubility of **ICG** is often quoted as 1 mg/mL and to ensure that all our studies used completely dissolved aqueous solutions we employed a consistent concentration of 1.0 mM (0.775 mg/mL). We discovered that the purity and composition of a 1.0 mM stock solution of **ICG** in water could be conveniently tracked over time by periodically removing a small aliquot and analyzing its chemical composition at a semi-quantitative level by reverse phase thin-layer chromatography (TLC),[48] or at a quantitative level using ^{1}H NMR spectroscopy.[27,28] We found that under normal clinical reconstitution and shelf-storage conditions, the oxidative dimerization of aqueous **ICG** to produce **1** (pathway C in Scheme 2) was by far the dominant degradation pathway and preparative experiments provided pure samples of **1**, [D_8]-**1**, and [D_{12}]-**1** whose ^{1}H NMR and mass spectra were internally consistent (Figures S2) and matched the literature data.[27,28,49] The first indication that a stored 1.0 mM solution of aqueous [D_5]-**ICG** was substantially more stable than a homologous solution of **ICG** was gained by monitoring stock solutions over one week at room temperature using reverse phase TLC (Figure S18). This finding was confirmed by comparing NMR spectra of aliquots taken periodically from the separate stored stock solutions (Figures S19 and S20). In Figure 1a, the changes over time are shown for one particularly diagnostic peak corresponding to the $-CH_2SO_3^-$ protons at $\delta = 2.91$ ppm for **ICG** or [D_5]-**ICG**, and $\delta = 2.80$ ppm for **1** or [D_8]-**1**. Comparison of peak integration

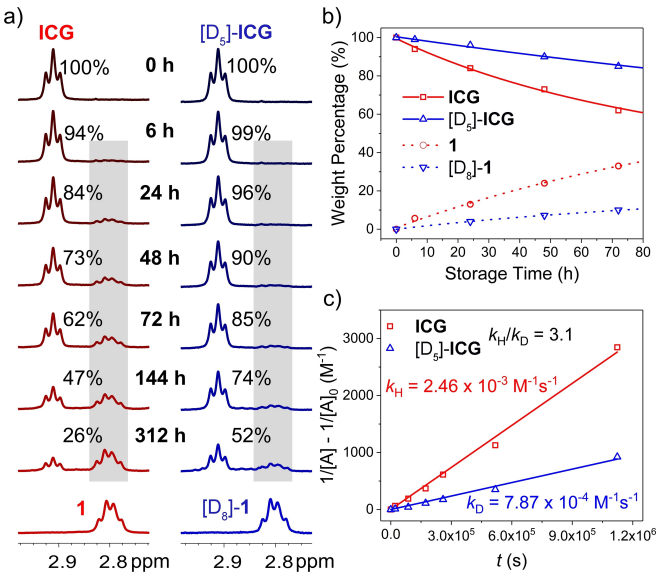

Figure 1. a) Partial ^{1}H NMR spectra (500 MHz, [D_4]methanol, 25 °C) showing differences in stability for separate stock solutions of **ICG** or [D_5]-**ICG** in water (1.0 mM) at room temperature. The spectra show a decrease in the peak for $-CH_2SO_3^-$ protons at $\delta = 2.91$ ppm for **ICG** or [D_5]-**ICG** and an increase in the corresponding peak at $\delta = 2.80$ ppm for oxidative dimer **1** or [D_8]-**1**. b) Speciation plots showing the change in weight percentage with storage time. Each plot was fit to a pseudo-second-order dimerization reaction model. c) Curve fitting of the data to give the ratio of rate constants (k_H/k_D) as a deuterium kinetic isotope effect in water (1.0 mM) at room temperature (22 °C).

values with an internal NMR standard (CH_3SO_3Na, $\delta = 2.69$ ppm) produced kinetic plots (Figure 1b, with expanded time plot in Figure S21) that could be analyzed to provide second-order rate constants for the bimolecular dimerization reaction to form **1** (or [D_8]-**1**; Figure 1c).

The ratio of rate constants (deuterium kinetic isotope effect) shows that the conversion of aqueous [D_5]-**ICG** to [D_8]-**1** is slower than the conversion of **ICG** to **1** by a factor of 3.1. A subsequent kinetic study used the same NMR assay to quantify the conversion of [D_7]-**ICG** to oxidized dimer [D_{12}]-**1** and found that it matched the conversion rate of [D_5]-**ICG** to [D_8]-**1** (Figure S22 and Table S2).

Chemical implications

The scattered literature reports on **ICG** stability over several decades reflect a complicated dependence on light and solvent, and there is some previous evidence that **ICG** stability in water is moderately enhanced by higher concentration.[50] Repeated kinetic measurements on different batches of aqueous **ICG** (1.0 mM) under the same multiday storage and sampling conditions revealed a slight batch-to-batch variation in the rates of oxidative dimerization, likely reflecting minor differences in sample exposure to laboratory lighting. A systematic series of comparative experiments produced the following mechanistic observations.

1. The dimerization reaction to produce **1** was inhibited when air and/or light was excluded from the reaction (Figure S26). However, slow production of **1** continued after an illuminated sample of **ICG** was placed in the dark.
2. The dimerization reaction was strongly inhibited by the presence of additives that act as antioxidants, such as azide and ascorbate, but it was promoted by the presence of NaI an additive in some commercial versions of **ICG** (Figure S27).
3. There was less photochemical degradation when the concentration of **ICG** in water or ethanol was increased (Figures S16, S17, and S28b).
4. Under low photon intensity conditions, a stored solution of 1.0 mM **ICG** in water slowly produced **1** but an analogous solution of **ICG** in ethanol did not (Figure S28a).
5. The dimerization reaction to produce **1** under low photon intensity light conditions was enhanced when the aqueous solution of **ICG** (1.0 mM) included H_2O_2 (10 mM) (Figure S29).

The chemical analysis data clearly shows that the dominant degradation pathway for a stored clinical formulation of aqueous **ICG** (1.0–2.5 mg/mL) is oxidative dimerization to produce **1**. The observed deuterium kinetic isotope effect of 3.1 with [D_5]-**ICG** (or [D_7]-**ICG**) is consistent with the reaction mechanism proposed by Rüttger and co-workers,[27] although significant new insight is provided by the experimental observations listed above. The new chemical insight can be summarized as four major points.

1. The high optical density of a clinical formulation produces a very strong inner filter effect that stops light reaching the dye molecules located deep in the solution, thus attenuating **ICG** photobleaching by any mechanism (Figures S16, S17, and S28b).
2. There is extensive self-association of **ICG** in water to form face-to-face H-aggregates that favor rapid quenching of dye excited states,[8,51] This aggregation-induced quenching reinforces the inner filter effect to further slow photobleaching of a clinical **ICG** formulation in water.
3. As summarized in Scheme 4a, the dominant reaction of a monomeric **ICG** molecule and photosensitized singlet oxygen is cycloaddition with the heptamethine and subsequent fragmentation of the dioxetane intermediates to produce carbonyl-containing fragments (pathway A in Scheme 2). A major finding of this work is an aggregation-induced switch in **ICG** photoreactivity towards a path that produces the oxidative dimer **1** (pathway C in Scheme 2). As summarized in Scheme 4b, a tightly packed H-aggregate sterically hinders attack of singlet oxygen at the polymethine double bonds, and concomitantly favors photosensitized oxidative dimerization by promoting the covalent coupling of an **ICG** radical cation with an adjacent **ICG** molecule in the same aggregate.[52] This picture of aggregation-dependent reactivity is supported by experiments in organic solvents, such as ethanol, where there is negligible **ICG** self-aggregation and very little oxidative dimerization (Figure S28a). There is also recent literature evidence that self-aggregation in water promotes photoinduced electron transfer from **ICG** to molecular oxygen.[53]

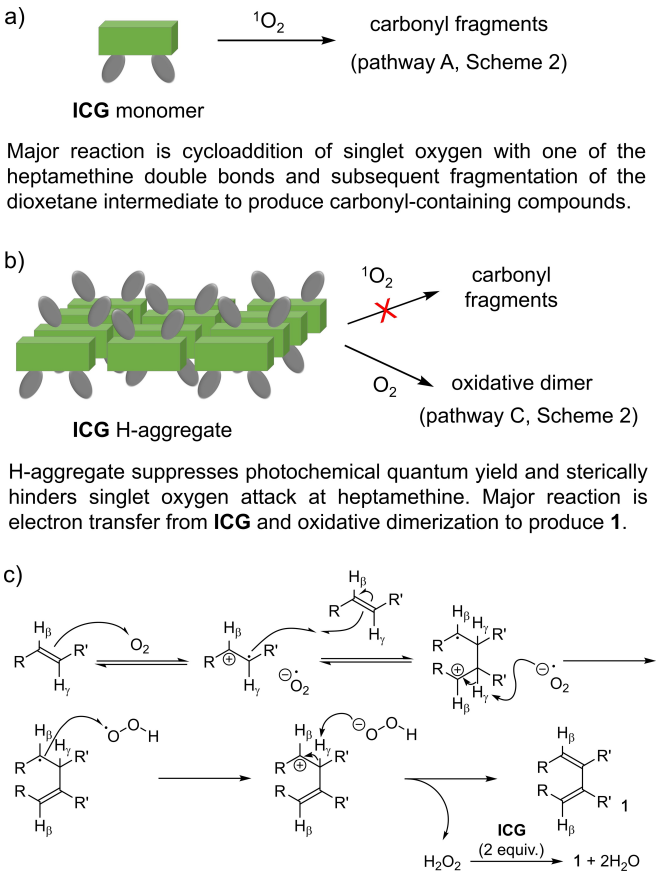

Scheme 4. Different major pathways for reaction of: a) **ICG** monomer with photosensitized singlet oxygen in any solvent, or b) excited state **ICG** in H-aggregate with molecular oxygen. c) Proposed mechanism for photosensitized oxidative dimerization of **ICG** to form **1**.[27,54]

4. The first two steps in the proposed photosensitized oxidative dimerization mechanism in Scheme 4c involve reversible electron transfer from excited triplet state **ICG** to dissolved molecular oxygen to produce a superoxide radical anion and **ICG** radical cation, followed by reversible attack of the radical cation on a second **ICG** molecule.[23,27,47,53–56] Subsequent proton abstraction is an irreversible third step that is slowed in [D_5]-**ICG** (and also in [D_7]-**ICG**) because the activation energy for deuteron abstraction is higher. These three steps rationalize the observed deuterium kinetic isotope effect of 3.1 and also the observed second order dependence on [**ICG**] (see Figure S30 for expanded kinetic expression). Hydrogen peroxide is a reaction by-product that subsequently dimerizes two additional **ICG** molecules in a light-independent manner;[57] and thus the oxidative dimer **1** continues to be slowly produced after an illuminated clinical dose of aqueous **ICG** is stored in the dark. In terms of reaction stoichiometry, one singlet oxygen molecule converts four molecules of **ICG** into two molecules of **1**.

Clinical implications

The oxidative dimer **1** has a similar NIR absorption spectrum as **ICG** but the fluorescence quantum yield is ~100-fold lower (Table 1) and as shown in Figures S9 and S10, compound **1** emits virtually no fluorescence. The very low fluorescence quantum yield is consistent with that reported for an analogous oxidized dimer of a pentamethine cyanine dye,[58] and an energy minimized molecular model of **1** (Figure S31) reveals a highly twisted 3D shape with the two connected heptamethines oriented almost orthogonally. Compared to **ICG** there is little change in the absorption maxima band indicating very weak coupling of the polymethine transition state dipoles, but there is efficient intramolecular energy transfer and nonradiative decay of the excited state. In terms of fluorescence imaging, oxidized dimer **1** is a NIR light-absorbing but non-fluorescent product of **ICG** degradation that builds up during storage of a clinical aqueous formulation and lowers the image brightness produced by the dose. To illustrate the difference in image brightness due to the change in stock solution stability, we conducted an NIR fluorescence imaging study that compared two mouse phantoms with fillable organs (Figures 2 and S31). To mimic a typical **ICG** in vivo imaging scenario, the heart port of each phantom mouse was filled with FBS and an aliquot from a 1.0 mM stock solution of either **ICG** or [D_5]-**ICG** (final dye concentration was 2 μM). NIR fluorescence images were acquired using an animal imaging station and the mean pixel intensities of the heart regions where determined. When the experiment used fresh stock solutions there was no difference in image intensities for the phantoms containing **ICG** or [D_5]-**ICG**, which is consistent with the matching fluorescence brightness observed when the dyes are in serum (Table 1). But when the imaging experiment was repeated using aliquots from stock solutions that had been stored in the dark for 3 days, the image intensity of the heart region containing **ICG** was 80% of the image intensity of the heart region filled with [D_5]-**ICG**. TLC analysis of the stock solutions showed that conversion into non-fluorescent **1** was the primary reason for the decreased **ICG** image intensity (Figure S31). Undoubtedly, the difference in NIR fluorescent image intensities would be even larger if the aqueous stock solutions were stored for longer periods or if they were exposed to more light during preparation and storage.

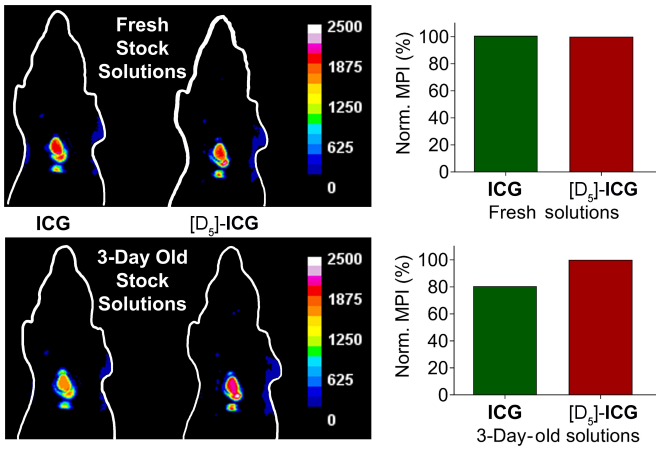

Figure 2. NIR fluorescence images (λ_{ex}: 745 nm, λ_{em}: 850 nm) of two mouse phantoms with heart portals containing FBS and an aliquot from a 1.0 mM aqueous stock solution of either **ICG** or [D_5]-**ICG** (final dye concentration, 2 μM). The top pair of phantoms contain freshly prepared stock solutions and the bottom pair contain 1.0 mM aqueous stock solutions that had been stored for 3 days at room temperature (22 °C). The fluorescence intensity scale is in arbitrarily units. The graphs compare normalized mean pixel intensity (MPI) for the fluorescent heart regions within each pair of mouse phantom images. The graph error bars are too small to visualize.

One of the key pharmaceutical properties of **ICG** is its high affinity for blood proteins which ensures that it does not leave the vasculature of a living subject. Compared to **ICG**, the oxidative dimer **1** exhibits a higher retention factor (R_f value) on a reversed phase TLC plate, indicating a more polar molecular structure; this is consistent with the molecular model in Figure S32 showing a dispersed projection of the four anionic sulfonate groups. The combination of polyanionic charge and nonplanar shape suggested to us that **1** would likely have relatively low affinity for blood proteins,[59] and this supposition was confirmed by measuring dissociation constants for binding to bovine serum albumin in pH 7.4 PBS buffer at 37 °C (Figures S11–S14). The measured values of K_d for **ICG**, [D_5]-**ICG**, [D_7]-**ICG** were all within measurement error of 2.9 μM which is close to the literature value for **ICG**.[59] In contrast, the K_d for **1** was ten-fold higher at 34 μM which means if **1** was present in the blood at the low micromolar dose concentrations that are typically employed for clinical imaging, hardly any of it would be associated with high molecular weight albumin protein. Thus, there is high potential for polar **1** to extravasate from the bloodstream,[59] and a goal of future work is to determine if **1** induces any undesired pharmaceutical effects as a storage degradation product of **ICG**. For example, the structure of **1** suggests that it might be an inhibitor of the organic anion transporters that mediate renal clearance of many environmental toxins or clinically important drugs.[60]

Since **ICG** is excreted chemically unchanged into the intestines, it is very unlikely that [D_5]-**ICG** (or [D_7]-**ICG**) will exhibit any significant difference in clinical pharmacokinetics or in vivo imaging performance.[14,15] The longer shelf-life of aqueous [D_5]-**ICG** (or [D_7]-**ICG**) is an attractive clinical prospect for several reasons. It means that multiple doses can be drawn from a single large stock solution of aqueous [D_5]-**ICG** (or [D_7]-**ICG**) and used for a multi-dose imaging procedure with the reassurance that the purity of a carefully stored stock solution will not change significantly over several days at room temperature. In particular, multi-dose surgical procedures using **ICG** would be simplified and shortened if all the doses could be drawn from a single stock solution.[14] Not surprisingly, the shelf-life of an **ICG** stock solution is extended significantly when stored in the dark at 4 °C in a refrigerator. As shown in Figure S23, the purity of an aqueous solution of **ICG** (1.0 mM) was 85 and 52% after 7 and 28 days' storage at 4 °C in the dark, whereas the purity of an analogous stored sample of [D_5]-**ICG** (1.0 mM) was 95 and 85% after the same storage times. The enhanced shelf-life of refrigerated stock solutions of [D_5]-**ICG** will make it very convenient and economical for longitudinal

preclinical in vivo imaging studies that need to repeatedly dose a large cohort of animals over a long period of time.[61,62]

Conclusions

Indocyanine Green (**ICG**) has been used extensively as a clinically approved NIR fluorescent dye for more than 60 years. While **ICG** is reasonably stable when associated with proteins in the bloodstream, its propensity to degrade as a concentrated aqueous stock solution means that clinical doses have to be used shortly after reconstitution. The results of this study show that self-aggregation of **ICG** in water favors dye degradation by a photochemical oxidative dimerization reaction that gives the nonfluorescent product **1**. [D_5]-**ICG** and [D_7]-**ICG** are deuterated versions of **ICG** with deuterium atoms on the heptamethine chain, and storage stability studies show that the replacement of C–H with C–D decreases the dimerization rate constant by a factor of 3.1. All three homologues have the same affinity for albumin protein and produce noncovalent complexes with the same fluorescence brightness. As **ICG** is excreted unchanged from the body, it is very likely that [D_5]-**ICG** and [D_7]-**ICG** will exhibit the same clinical performance. But the extended storage shelf-lives of aqueous [D_5]-**ICG** and [D_7]-**ICG** will improve many biomedical imaging and diagnostic procedures, including fluorescence-guided surgeries that draw repeated doses from the same stock solution over a lengthy period of time. From a broader biomedical perspective, the results of this study suggest additional future research directions for pursuit. For example, the idea that self-aggregation of amphiphilic cyanine dyes, like **ICG**, can promote photoinduced electron transfer chemistry has been recognized by dye chemists for some time,[63] but has not yet been fully exploited as a rational design paradigm for next-generation photodynamic therapy.[53,64] Likewise, deuterated polymethine cyanine dyes with a low propensity for photooxidative dimerization are promising future candidates for optimized super-resolution microscopy.[65]

Acknowledgements

We are grateful for funding support from the US NIH (R35GM136212). We thank Rananjaya S. Gamage for conducting the mouse phantom imaging experiments.

Keywords: cyanines · deuterium · dyes/pigments · fluorescent probes · imaging agents

[1] L. van Manen, H. J. M. Handgraaf, M. Diana, J. Dijkstra, T. Ishizawa, A. L. Vahrmeijer, J. S. D. Mieog, *J. Surg. Oncol.* **2018**, *118*, 283–300.
[2] M. B. Reinhart, C. R. Huntington, L. J. Blair, B. T. Heniford, V. A. Augenstein, *Surg. Innov.* **2016**, *23*, 166–175.
[3] T. Desmettre, J. M. Devoisselle, S. Mordon, *Surv. Ophthalmol.* **2000**, *45*, 15–27.
[4] J. T. Alander, I. Kaartinen, A. Laakso, T. Pätilä, T. Spillmann, V. V. Tuchin, M. Venermo, P. Välisuo, *Int. J. Biomed. Imaging* **2012**, *2012*, 7.
[5] M. Mazurek, B. Kulesza, F. Stoma, J. Osuchowski, S. Mańdziuk, R. Rola, *Diagnostics* **2020**, *10*, 1100.
[6] A. Rozenholc, V. Samouelian, T. Warkus, P. Gauthier, D. Provencher, P. Sauthier, F. Gauthier, P. Drakopoulos, B. Cormier, *Gynecol. Oncol.* **2019**, *153*, 500–504.
[7] B. K. Byrd, M. Marois, K. M. Tichauer, D. J. Wirth, J. Hong, J. P. Leonor, J. T. Elliott, K. D. Paulsen, S. C. Davis, *J. Biomed. Opt.* **2019**, *24*, 080501.
[8] E. D. Cosco, I. Lim, E. M. Sletten, *ChemPhotoChem* **2021**, *5*, 727–734.
[9] E. P. Porcu, A. Salis, E. Gavini, G. Rassu, M. Maestri, P. Giunchedi, *Biotechnol. Adv.* **2016**, *34*, 768–789.
[10] M. Hope-Ross, L. A. Yannuzzi, E. S. Gragoudas, D. R. Guyer, J. S. Slakter, J. A. Sorenson, S. Krupsky, D. A. Orlock, C. A. Puliafito, *Ophthalmology* **1994**, *101*, 529–533.
[11] J. Gathje, R. R. Steuer, K. R. Nicholes, *J. Appl. Physiol.* **1970**, *29*, 181–185.
[12] S. Yoneya, T. Saito, Y. Komatsu, I. Koyama, K. Takahashi, J. Duvoll-Young, *Investig. Ophthalmol. Vis. Sci.* **1998**, *39*, 1286–1290.
[13] J. Fengler, *Colorectal Dis.* **2015**, *17*, 3–6.
[14] N. M. Fanaropoulou, A. Chorti, M. Markakis, M. Papaioannou, A. Michalopoulos, T. Papavramidis, *Medicine* **2019**, *98*, e14765.
[15] E. Levesque, E. Martin, D. Dudau, C. Lim, G. Dhonneur, D. Azoulay, *Anaesth. Crit. Care Pain Med.* **2016**, *35*, 49–57.
[16] E. Kaplan-Marans, J. Fulla, N. Tomer, K. Bilal, M. Palese, *Urology* **2019**, *132*, 10–17.
[17] S. S. Cho, V. P. Buch, C. W. Teng, E. De Ravin, J. Y. K. Lee, *World Neurosurg.* **2020**, *136*, 326.
[18] C. W. Teng, V. Huang, G. R. Arguelles, C. Zhou, S. S. Cho, S. Harmsen, J. Y. K. Lee, *Neurosurg. Focus* **2021**, *50*, E4.
[19] R. Zeh, S. Sheikh, L. Xia, J. Pierce, A. Newton, J. Predina, S. Cho, M. Nasrallah, S. Singhal, J. Dorsey, J. Y. K. Lee, *PLoS One* **2017**, *12*, e0182034.
[20] P. L. Rappaport, J. J. Thiessen, *J. Pharm. Sci.* **1982**, *71*, 157–161.
[21] R. Rajagopalan, P. Uetrecht, J. E. Bugaj, S. A. Achilefu, R. B. Dorshow, *Photochem. Photobiol.* **2000**, *71*, 347–350.
[22] J. M. I. Maarek, D. P. Holschneider, J. Harimoto, *J. Photochem. Photobiol. B* **2001**, *65*, 157–164.
[23] R. R. Nani, J. A. Kelley, J. Ivanic, M. J. Schnermann, *Chem. Sci.* **2015**, *6*, 6556–6563.
[24] E. Engel, R. Schraml, T. Maisch, K. Kobuch, B. Konig, R. M. Szeimies, J. Hillenkamp, W. Baümler, R. Vasold, *Investig. Ophthalmol. Vis. Sci.* **2008**, *49*, 1777–1783.
[25] D. A. Helmerich, G. Beliu, S. S. Matikonda, M. J. Schnermann, M. Sauer, *Nat. Methods* **2021**, *18*, 253–257.
[26] S. S. Matikonda, D. A. Helmerich, M. Meub, G. Beliu, P. Kollmannsberger, A. Greer, M. Sauer, M. J. Schnermann, *ACS Cent. Sci.* **2021**, *7*, 1144–1155.
[27] F. Rüttger, S. Mindt, C. Golz, M. Alcarazo, M. John, *Eur. J. Org. Chem.* **2019**, *2019*, 4791–4796.
[28] S. Mindt, I. Karampinis, M. John, M. Neumaier, K. Nowak, *Photochem. Photobiol. Sci.* **2018**, *17*, 1189–1196.
[29] S. Cargnin, M. Serafini, T. Pirali, *Future Med. Chem.* **2019**, *11*, 2039–2042.
[30] N. J. Turro, V. Ramamurthy, J. C. Scaiano, *Principle of Molecular Photochemistry*, University Science Books: Sausalito, **2009**, pp. 304.
[31] J. B. Grimm, L. Xie, J. C. Casler, R. Patel, A. N. Tkachuk, N. Falco, H. Choi, J. Lippincott-schwartz, T. A. Brown, B. S. Glick, Z. Liu, L. D. Lavis, *JACS* **2021**, *1*, 690–696.
[32] K. Kolmakov, V. N. Belov, J. Bierwagen, C. Ringemann, V. Müller, C. Eggeling, S. W. Hell, *Chem. Eur. J.* **2010**, *16*, 158–166.
[33] M. Lipowska, S. E. Patterson, G. Patonay, L. Strekowski, *J. Heterocycl. Chem.* **1993**, *30*, 1177–1180.
[34] K. Kundu, S. F. Knight, S. Lee, W. R. Taylor, N. Murthy, *Angew. Chem. Int. Ed.* **2010**, *49*, 6134–6138; *Angew. Chem.* **2010**, *122*, 6270–6274.
[35] L. Štacková, P. Štacko, P. Klán, *J. Am. Chem. Soc.* **2019**, *141*, 7155–7162.
[36] L. Štacková, E. Muchová, M. Russo, P. Slavíček, P. Štacko, P. Klán, *J. Org. Chem.* **2020**, *85*, 9776–9790.
[37] O. A. Okoh, R. H. Bisby, C. L. Lawrence, C. E. Rolph, R. B. Smith, *J. Sulfur Chem.* **2014**, *35*, 42–56.
[38] G. E. Ficken, J. D. Kendall, *J. Chem. Soc.* **1959**, 3988–3992.
[39] I. Yamaguchi, A. Kado, T. Fukuda, H. Fukumoto, T. Yamamoto, M. Sato, *Eur. Polym. J.* **2010**, *46*, 1119–1130.
[40] J. Kuthan, J. Krechl, M. Belohradsky, *Collect. Czech. Chem. Commun.* **1982**, *47*, 3283–3287.
[41] J. Becher, M. C. Christensen, *Tetrahedron* **1979**, *35*, 1523–1530.
[42] A. P. Gorka, R. R. Nani, M. J. Schnermann, *Org. Biomol. Chem.* **2015**, *13*, 7584–7598.
[43] A. P. Demchenko, *Methods Appl. Fluoresc.* **2020**, *8*, 022001.
[44] J.-Y. Koo, G. B. Schuster, *J. Am. Chem. Soc.* **1975**, *99*, 5403–5408.
[45] V. Saxena, M. Sadoqi, J. Shao, *J. Pharm. Sci.* **2003**, *92*, 2090–2097.

[46] W. Holzer, M. Mauerer, A. Penzkofer, R. M. Szeimies, C. Abels, M. Landthaler, W. Bäumler, *J. Photochem. Photobiol. B* **1998**, *47*, 155–164.
[47] X. Zhang, M. A. J. Rodgers, *J. Phys. Chem.* **1995**, *99*, 12797–12803.
[48] F. Barbier, G. A. Deweerdt, *Clin. Chim. Acta* **1964**, *10*, 549–554.
[49] Inspection of the ^{1}H NMR spectra for samples of aqueous **ICG** stored at room temperature for extended periods (Figure S19) showed that the combined mass balance of **ICG** and **1** was >95% of the dye-derived species. Mass spectral analysis of the samples indicated that the remaining mass balance was a mixture of the other compounds shown in Scheme 2, namely, the carbonyl-containing compounds and truncated pentamethine homologue. The latter compound was isolated and exhibited NMR and mass spectra that matched the literature (Figure S25).
[50] J. F. Zhou, M. P. Chin, S. A. Schafer, *Proc. SPIE* **1994**, *2128*, 495–505.
[51] H. V. Berlepsch, C. Böttcher, *J. Phys. Chem. B* **2015**, *119*, 11900–11909.
[52] Freshly prepared solutions of concentrated **ICG** in water immediately form face-to-face stacked H-aggregates but upon room temperature storage over ~2 weeks there is a morphological change to J-aggregates with head-to-tail packing. See, M. L. Landsman, G. Kwant, G. A. Mook, W. G. Zijlstra, *J. Appl. Physiol.* **1976**, *40*, 575–583. It seems unlikely that this very slow change in **ICG** aggregate morphological has any impact on the photochemistry described in Scheme 4.
[53] H. Fan, Y. Fan, W. Du, R. Cai, X. Gao, X. Liu, H. Wang, L. Wang, X. Wu, *Nanoscale* **2020**, *12*, 9517–9523.
[54] The mechanistic data does not preclude the possibility that **1** forms by bimolecular coupling of two **ICG** radical cations followed by deprotonation, a process that would likely be promoted by **ICG** aggregation in water.
[55] C. Chen, B. Zhou, D. Lu, G. Xu, *J. Photochem. Photobiol. A* **1995**, *89*, 25–29.
[56] R. L. Parton, J. R. Lenhard, *J. Org. Chem.* **1990**, *55*, 49–57.
[57] T. C. Barros, S. H. Toma, H. E. Toma, E. L. Bastos, M. S. Baptista, *J. Phys. Org. Chem.* **2010**, *23*, 893–903.
[58] S. Miltsov, V. Karavan, A. Misharev, G. Starova, J. Alonso-Chamarro, M. Puyol, *Tetrahedron Lett.* **2017**, *58*, 3353–3357.
[59] M. Y. Berezin, K. Guo, W. Akers, J. Livingston, M. Solomon, H. Lee, K. Liang, A. Agee, S. Achilefu, *Biochemistry* **2011**, *50*, 2691–2700.
[60] P. Duan, S. Li, N. Ai, L. Hu, W. J. Welsh, G. You, *Mol. Pharm.* **2012**, *9*, 3340–3346.
[61] N. Onda, M. Kimura, T. Yoshida, M. Shibutani, *Int. J. Cancer* **2016**, *139*, 673–682.
[62] It is worth noting that **ICG** degradation is inhibited by the presence of antioxidant additives such as azide or ascorbate (Figure S27), but **ICG** formulations with stabilizing additives are not clinically approved due to the increased risk of patient side effects. In contrast, a formulation of pure [D_5]-**ICG** (or [D_7]-**ICG**) in sterile water is more likely to be a safe clinical replacement of **ICG** in water. Of course, if an additive is eventually found to safely stabilize **ICG**, then the shelf-life of a clinical dose can likely be extended an additional three times by using [D_5]-**ICG** (or [D_7]-**ICG**).
[63] S. Kirstein, S. Daehne, *Int. J. Photoenergy* **2006**, *2006*, 20363.
[64] M. Sevieri, F. Silva, A. Bonizzi, L. Sitia, M. Truffi, S. Mazzucchelli, F. Corsi, *Front. Chem.* **2020**, *8*, 1–9.
[65] A. Lisovskaya, I. Carmichael, A. Harriman, *J. Phys. Chem. A* **2021**, *125*, 5779–5793.

Manuscript received: August 2, 2021
Accepted manuscript online: August 17, 2021
Version of record online: September 24, 2021

